Application of Stochastic Finite Element Methods to Study the Sensitivity of ECG Forward Modeling to Organ Conductivity

Sarah E. Geneser, Robert M. Kirby*, *Member, IEEE*, and Robert S. MacLeod, *Member, IEEE*

***Abstract*—Because numerical simulation parameters may significantly influence the accuracy of the results, evaluating the sensitivity of simulation results to variations in parameters is essential. Although the field of sensitivity analysis is well developed, systematic application of such methods to complex biological models is limited due to the associated high computational costs and the substantial technical challenges for implementation. In the specific case of the forward problem in electrocardiography, the lack of robust, feasible, and comprehensive sensitivity analysis has left many aspects of the problem unresolved and subject to empirical and intuitive evaluation rather than sound, quantitative investigation. In this study, we have developed a systematic, stochastic approach to the analysis of sensitivity of the forward problem of electrocardiography to the parameter of inhomogeneous tissue conductivity. We apply this approach to a two-dimensional, inhomogeneous, geometric model of a slice through the human thorax. We assigned probability density functions for various organ conductivities and applied *stochastic finite elements* based on the generalized polynomial chaos-stochastic Galerkin (gPC-SG) method to obtain the standard deviation of the resulting stochastic torso potentials. This method utilizes a spectral representation of the stochastic process to obtain numerically accurate stochastic solutions in a fraction of the time required when employing classic Monte Carlo methods. We have shown that a systematic study of sensitivity is not only easily feasible with the gPC-SG approach but can also provide valuable insight into characteristics of the specific simulation.**

***Index Terms*—Electrocardiographic forward problem, polynomial chaos, stochastic finite elements, stochastic Galerkin, stochastic processes, uncertainty quantification.**

I. Introduction

THE forward problem of electrocardiography provides valuable information for both basic science and clinical medicine and has a well-established set of solution approaches [1]–[3]. Computational electrocardiographic models based on realistic human physiology include many input parameters, such as the geometric discretization of the torso organs, the conductivities of the tissues, and the representation of cardiac sources. Inherent in each model parameter are "errors" associated with quantifying and simplifying the physiology so that numerical implementations remain tractable. These errors can result, for example, from simplifications or abstractions of the physics or geometry (modeling errors), lack of instrumentation precision in obtaining model parameters (parameter errors) as well as from natural variations over patient populations. Quantification and control of such errors are critical to the simulation process; only then can scientists judiciously evaluate which components of the model are critically sensitive to variations and hence may require additional refinement or more accurate measurements. In the specific case of the electrocardiographic forward problem, tissue conductivity is an example of an input parameter that is very difficult to accurately obtain; establishing conductivity in realistic conditions requires careful experiments and complex interpretation with often widely varying results [4]–[6]. The role of such variations in conductivity on simulations is the topic of extensive ongoing research and discussion, with no obvious means of resolution available [7]–[13].

The goal of this study was to present and show the utility of a novel methodology of sensitivity analysis first presented in [14]–[16] that is applicable to a wide range of problem in bioelectric fields. To demonstrate its feasibility, we utilized the approach to evaluate the effects of variations and uncertainty in the conductivity values assigned to organs in a two-dimensional model of the human thorax. The mathematical framework presented herein extends naturally for use on three-dimensional models; we focus on a two-dimensional model for the sake of clarity of presentation.

Sensitivity analysis in computational modeling provides a quantitative description of the dependence of the solution on various model parameters and input values. Such analysis can provide insight into the relative impact of parameter variation on solution accuracy, which, in turn, has implications regarding the underlying mechanisms of the model system. Sensitivity analysis methods were first developed for the assessment of mathematical models of control systems [17]–[19] and have a strong tradition in the analysis of mechanical systems [20]. However, the value of the sensitivity approach extends beyond these initial applications. The approach is especially useful for biological systems as they typically require a high level

Manuscript received November 22, 2006; revised April 18, 2007. This work was funded by a University of Utah Seed Grant Award, NSF Career Award (Kirby) NSF-CCF0347791, and the NIH NCRR Center for Integrative Biomedical Computing (www.sci.utah.edu/cibc), NIH NCRR Grant 5P41RR012553-02. *Asterisk indicates corresponding author*.

S. E. Geneser is with the School of Computing and Scientific Computing and Imaging Institute, University of Utah, Salt Lake City, UT 84112 USA (e-mail: geneser@cs.utah.edu).

*R. M. Kirby is with the School of Computing and Scientific Computing and Imaging Institute, University of Utah, Salt Lake City, UT 84112 USA (e-mail: kirby@cs.utah.edu).

R. S. MacLeod is with the Department of Bioengineering and the Nora Eccles Harrison Cardiovascular Research and Training Institute, University of Utah, Sale Lake City, UT 84112 USA (e-mail: macleod@cvrti.utah.edu).

Digital Object Identifier 10.1109/TBME.2007.900563

of simplification and abstraction to encapsulate physiological mechanisms in tractable simulations. Many parameters in biological simulations are approximations based on experiments and in many cases, the interplay between such parameter approximations and other modeling assumptions is not clear. Such an approach can identify aspects of the model that may be simplified or reduced without significantly impacting the solution accuracy.

Several methods for carrying out sensitivity analysis exist, but they are not widely applied to complex systems due to their computational cost and difficulty of implementation. For example, sampling-based sensitivity methods such as Monte Carlo [21], [22], Latin Hypercube [23], [24], response surface [25], reliability-based methods [26], [27], and the Fourier amplitude sensitivity test [28] are often impractical due to the large number of repetitions necessary to obtain statistically valid results. The time required to compute sufficient samples for accurate solutions often forces researchers to revert to highly undersampled "brute-force" methods [29], [30]. Sometimes referred to as "sensitivity testing," this technique investigates the model response to an extremely reduced set of model parameter combinations, and thus fails to provide robust quantification of the model sensitivity.

Several methods exist to directly calculate sensitivity coefficients rather than to extract them from large numbers of test simulations. One scheme is based on the coupled direct method in which the model equations are differentiated with respect to the parameters of interest and the resulting set of sensitivity equations is solved simultaneously with the model equations [31]. Another class of techniques relies on the Green's function or adjoint method, also based on differentiation of the model equations. In this case, one constructs an auxiliary set of Green's functions thus minimizing the number of differential equations that must then be solved to obtain sensitivity coefficients [32], [33]. Examples of differential analysis methods include the Neumann [34] and Taylor series [35], [36] expansions, and perturbation analysis [37]–[39]. These methods are computationally efficient, but require that the perturbation terms be small, i.e., only limited variations in parameters are possible, and can be very cumbersome to apply to complex simulations. Moreover, for nonlinear systems, the resulting equations for these analytical methods can be mathematically intractable.

In summary, most sensitivity analysis techniques to date have suffered from one of the following limitations: 1) they are expensive to compute (in comparison with solving the single deterministic model problem); 2) they require extensive mathematical adaptation or manipulation of the original model (such as computing Fréchet derivatives of an already complex system); or 3) they restrict the range of parameter or model perturbations in a way that hampers one's ability to answer the sensitivity questions of interest.

In contrast to all the approaches described above, the generalized polynomial chaos-stochastic Galerkin (gPC-SG) technique attempts to alleviate these limitations by treating the input data and model parameters as stochastic processes and solving the resulting stochastic computational system of equations in order to obtain information about the sensitivity of the system. To accomplish this, it is necessary to assume a particular probability density function (PDF) for the parameters of interest, which arguably allows for even more subtlety in the sensitivity analysis. Once the stochastic solution is obtained through an orchestrated combination of deterministic model solutions, one can compute and examine the standard deviation and higher statistical moments of the result. Such information provides a quantitative description of the sensitivity and uncertainty of the system to the parameters.

Based on the Wiener–Hermite polynomial chaos expansion [40], gPC has been applied to a range of problems in computational mechanics [41]–[49]. This technique has also recently been introduced into other disciplines such as thermodynamics [50]–[52] and physical chemistry [53], [54], in part because it leads to efficient solutions to stochastic problems of interest, i.e., not only parameter sensitivity and uncertainty quantification.

To improve the computational efficiency of this method, we employ the stochastic Galerkin method to solve a generalized polynomial chaos representation of the stochastic system. The stochastic Galerkin method represents stochastic processes via orthogonal polynomials of random variables and utilizes specific sets of orthogonal polynomials to achieve computationally efficient representation of random processes with arbitrary probability density functions. Such expansions exhibit fast convergence rates when the stochastic response of the system is sufficiently smooth in the random space, e.g., bifurcation behavior is absent. The stochastic Galerkin method is an efficient means of reducing the stochastic governing equations to a system of deterministic equations that can then be solved via conventional numerical techniques.

We present here a development of the stochastic Galerkin method adapted to the forward problem of electrocardiography. With this approach it is possible to carry out a Galerkin projection of the governing equations onto the polynomials basis functions defined by gPC. Such a gPC-SG approach is capable of both applying relatively large perturbations in the model parameters and tolerating large variations in the responses. This method has been successfully applied to model uncertainty in complex stochastic solid and fluid problems [47], [48], [55] and is especially well suited to electrocardiographic forward problems because they are linear with relatively well behaved solutions. In this study, we demonstrated the feasibility of the gPC-SG approach by successfully applying it to a realistic two-dimensional model of the electrocardiographic forward problem. The results of this evaluation support some previous findings using other, less complete sensitivity studies but also suggest some new criteria for the creation of geometric models for bioelectric field problems.

II. Methods

The methods section is partitioned into two subsections, Section II-A outlines the standard approach we adopted for the electrocardiographic forward problem while Section II-B describes application of the gPC-SG technique to the standard ECG forward problem.

A. Electrocardiographic Forward Problem

The electrocardiographic forward problem is a quasi-static approximation of Maxwell's equations expressed as follows:

$$\nabla \cdot (\sigma(\boldsymbol{x})\nabla u(\boldsymbol{x})) = 0, \quad \boldsymbol{x} \in \Omega \tag{1}$$

$$u(\boldsymbol{x}) = u_0(\boldsymbol{x}), \quad \boldsymbol{x} \in \Gamma_D \tag{2}$$

$$\vec{n} \cdot \sigma(\boldsymbol{x})\nabla u(\boldsymbol{x}) = 0, \quad \boldsymbol{x} \in \Gamma_N \tag{3}$$

where Ω denotes the torso domain, Γ_D and Γ_N denote the epicardial (Dirichlet) and torso (Neumann) boundaries, respectively, $u(\boldsymbol{x})$ is the potential field on the domain Ω, $u_0(\boldsymbol{x})$ is the known epicardial potential boundary function, $\sigma(\boldsymbol{x})$ is the symmetric positive definite conductivity tensor, and $\vec{n}$ denotes the outward facing normal with respect to the torso.

1) Numerical Methodology: Solving (1)–(3) for any but the simplest geometries requires a numerical approximation, typically based on methods such as boundary elements or finite elements [1]. In order to facilitate the subsequent application of the stochastic Galerkin method, we employed a high-order finite-element method [56]–[58].

High-order elements refer to the polynomial order of the basis functions used to describe spatial variation of the variable(s) of interest. Basis functions with greater than first/linear degree provide a means of capturing more rapid variations in the system—and potentially achieving higher accuracy—without the need for refining the geometric mesh used to describe the domain under study. For this study, we first compared results using basis functions of first, second, and third degree and determined second degree to be adequate for all experimental results presented in this study.

We utilized a triangular tessellation $\mathcal{T}(\Omega)$ of the domain with the set $\mathcal{N}$ denoting indexes of the mesh nodes as the geometric basis for the finite element computations. For the case of linear finite elements, this set consisted of the indexes for the triangle vertices, and for the case of nodal high-order finite elements, the set contained indexes for nodes at the triangle vertices as well as the edge and internal discretization nodes. We then decomposed the set $\mathcal{N}$ into two nonintersecting sets, $\mathcal{B}$ and $\mathcal{I}$, representing nodal indexes that lie on the Dirichlet boundary (and hence denote positions at which the potentials are known) and nodal indexes for which the solution is sought (i.e., the N_{dof} degrees of freedom of the problem), respectively.

Let $\phi_i(\boldsymbol{x})$ denote the global finite element interpolating basis functions, which have the property that $\phi_i(\boldsymbol{x}_j) = \delta_{ij}$ where $\boldsymbol{x}_j$ denotes a node of the mesh for $j \in \mathcal{N}$. Solutions are then of the form:

$$u(\boldsymbol{x}) = \sum_{k \in \mathcal{N}} \hat{u}_k \phi_k(\boldsymbol{x}) \tag{4}$$

$$= \sum_{k \in \mathcal{I}} \hat{u}_k \phi_k(\boldsymbol{x}) + \sum_{k \in \mathcal{B}} \hat{u}_k \phi_k(\boldsymbol{x}) \tag{5}$$

where the first term of (5) denotes the sum over the degrees of freedom of the problem of the values at the unknown vertices weighted by the basis functions and the second term denotes the same sum for the (known) Dirichlet boundary conditions of the solution.

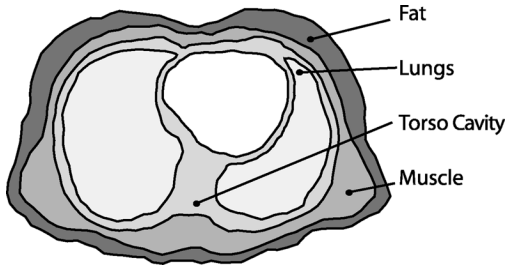

Fig. 1. Two-dimensional geometric model of the torso: Conductivity values were assigned according to the different regions of the torso slice which consisted of lungs, skeletal muscle, subcutaneous fat, and a miscellaneous category denoted torso cavity. Orientation of the slice is according to a standard radiological view, looking towards the head of a supine subject.

Substituting the expansion (5) into the differential (1), multiplying by a function from the test space $\{\phi_j(\boldsymbol{x}); j \in \mathcal{I}\}$, taking inner products, and integrating by parts yields a linear system of the form

$$\mathbf{S}\vec{u} = \vec{f} \tag{6}$$

where $\vec{u}$ denotes a vector containing the solution of the system (i.e., potential values at the nodal positions in $\mathcal{I}$) and $\mathbf{S}$ and $\vec{f}$ denote the stiffness matrix and right-hand-side function, respectively, given by the following expressions:

$$\mathbf{S} = S_{jk} = (\nabla\phi_j, \sigma\nabla\phi_k) \tag{7}$$

$$\vec{f} = f_j = \sum_{i \in \mathcal{B}} \hat{u}_i (\nabla\phi_j, \sigma\nabla\phi_i). \tag{8}$$

In the expressions above, $j, k \in \mathcal{I}$, and $(\cdot, \cdot)$ denote the inner product taken over the entire spatial domain Ω. Both the stiffness matrix and right-hand-side vector are functions of the conductivity. The stiffness matrix in (6) is positive definite, and hence solution of the linear system is amenable to iterative methods such as the preconditioned conjugate gradient method [59].

2) Geometric Model: The geometric model for this study consisted of a single two-dimensional slice of the Utah Torso Model [9], [60]. We adaptively refined the original mesh to achieve higher spatial density near the epicardial surface in order to improve numerical solution accuracy. Fig. 1 contains a diagram of the model showing regions representing lungs, skeletal muscle, subcutaneous fat, and a miscellaneous category denoted "torso cavity." The segmentation of the tissues ensured that boundaries always resided at the edges of elements and we assumed constant conductivity values over each organ region and hence within every element of that region. Although we did not consider anisotropy in this study, the model would easily support the assignment of conductivity tensors for each element.

3) Simulation Input Data: Boundary Conditions and Conductivity Parameters: Solving a particular case of the forward problem requires tissue conductivity values, which we obtained

TABLE I
CONDUCTIVITY VALUES CORRESPONDING TO ORGANS IN THE MODEL AND THE PERCENT AREA OF THE DOMAIN CONTRIBUTED

organ category	conductivity (S/m)	percent area of domain Ω
lungs	0.096	36.37%
skeletal muscle	0.200	22.93%
subcutaneous fat	0.045	21.61%
torso cavity	0.239	19.09%

from the literature [61] and summarized in Table I. Dirichlet boundary conditions took the form of potential values along the epicardial surface of the geometric model. For this, we utilized a set of potentials interpolated from 64-channel measurements performed on a human subject during open-chest ablation therapy for severe cardiac arrhythmia [61].

B. Sensitivity Quantification Through the Stochastic Galerkin Method

We now present the gPC-SG approach as applied to the ECG forward problem starting with a brief general overview of the gPC-SG formulation, followed by a description of our specific implementation of this methodology.

1) General Formulation: The stochastic Galerkin method represents any stochastic process $a(\boldsymbol{\xi})$ by a weighted sum of orthogonal polynomials [47], [48], [55], [62], which are functions of a vector of random variables $\boldsymbol{\xi}$ of known PDF. In the case of this study, the random processes of interest are the (stochastic) conductivity values attributed to different organs within the torso. The random variables of interest will be chosen to represent the distributions from which conductivity values are sampled. We denote the stochastic orthogonal polynomial set as $\psi_i(\boldsymbol{\xi})$ and can write

$$a(\boldsymbol{\xi}) = \sum_{i=0}^{\infty} \hat{a}_i \psi_i(\boldsymbol{\xi}). \tag{9}$$

For any reasonable random process, this infinite summation can be truncated to $P+1$ terms and the polynomial weights $\hat{a}_i$ are projections of the random input onto the random polynomials

$$\hat{a}_i = \int_{\Gamma} a(\boldsymbol{\xi})\psi_i(\boldsymbol{\xi})\mathrm{d}\mu = \langle a(\boldsymbol{\xi}), \psi_i(\boldsymbol{\xi})\rangle_{\mu} \tag{10}$$

in the stochastic domain Γ, where the random measure space μ is appropriate for the probability density function of the random variable vector $\boldsymbol{\xi}$. The stochastic coefficients of the trial expansion (as in the finite element method) are found by solving the resulting system for the random solution coefficients.

To apply this general approach to the specific case of an elliptical forward problem such as that in (1), we consider a stochastic conductivity tensor $\sigma(\boldsymbol{x};\boldsymbol{\xi})$ expressed in terms of an n-dimensional random variable vector $\boldsymbol{\xi} = (\xi_1, \xi_2, \ldots, \xi_n)^T$, where the PDFs of the random vector components are known or assumed. Because the conductivity tensors are physically constrained to be non-negative and nonzero, the PDF must be similarly constrained. The components of the random variable vector denote the different random variables necessary to describe the process of interest. When examining a stochastic process whose PDF is known, the smallest number of independent and uncorrelated random variables necessary to represent the process are typically obtained by such methods as Karhunen–Loeve (KL) expansion [63]. For example, if one were to model two tissue classes as stochastic and independent (in the statistical sense), a two-dimensional random variable vector would be utilized with the two components assigned to each tissue class respectively. The resulting stochastic versions of (1)–(3) are then

$$(\boldsymbol{\nabla}\cdot\sigma(\boldsymbol{x};\boldsymbol{\xi})\boldsymbol{\nabla})\,u(\boldsymbol{x};\boldsymbol{\xi}) = 0, \qquad \boldsymbol{x}\in\Omega \tag{11}$$

$$u(\boldsymbol{x};\boldsymbol{\xi}) = u_0(\boldsymbol{x};\boldsymbol{\xi}), \quad \boldsymbol{x}\in\Gamma_D \tag{12}$$

$$\vec{n}\cdot\sigma(\boldsymbol{x};\boldsymbol{\xi})\boldsymbol{\nabla}u(\boldsymbol{x};\boldsymbol{\xi}) = 0, \qquad \boldsymbol{x}\in\Gamma_N \tag{13}$$

where the solution $u(\boldsymbol{x};\boldsymbol{\xi})$ is now also a function of the stochastic variable vector $\boldsymbol{\xi}$ and thus has a random distribution with mean, variance, and higher stochastic moments. The conductivity tensor and solution field, as random processes, can be represented via the generalized stochastic Galerkin expansions as

$$u(\boldsymbol{x};\boldsymbol{\xi}) = \sum_{i=0}^{P} \tilde{u}_i(\boldsymbol{x})\psi_i(\boldsymbol{\xi}) \tag{14}$$

$$\sigma(\boldsymbol{x};\boldsymbol{\xi}) = \sum_{i=0}^{P} \tilde{\sigma}_i(\boldsymbol{x})\psi_i(\boldsymbol{\xi}) \tag{15}$$

where the functions $\psi_i(\boldsymbol{\xi})$ are orthogonal polynomials ranging up to Pth degree and P must be chosen to be large enough so that the solutions will meet the accuracy requirements for the particular system of interest. Convergence rates of the system depend on the choice of orthogonal polynomials for the underlying probability density functions of the random model parameter. Each probability distribution has a corresponding optimal set of orthogonal polynomials [62]; e.g., for Gaussian random functions, Hermite polynomials provide the best convergence, whereas the Legendre polynomials are best utilized for functions of uniform distributions, etc. When the stochastic response contains a discontinuity, e.g., near a bifurcation point, piecewise polynomials [64], [65] can be employed to circumvent the difficulty.

Substituting the above expressions into the stochastic elliptic system given by (11)–(13) and projecting (in the Galerkin sense) the resulting system into the random space spanned by the basis polynomials ψ_k leads to the following linear system:

For $k = 0, \ldots, P$

$$\sum_{i=0}^{P}\sum_{j=0}^{P} \mathcal{C}_{ijk}\boldsymbol{\nabla}\cdot(\tilde{\sigma}_i(\boldsymbol{x})\boldsymbol{\nabla}\tilde{u}_j(\boldsymbol{x})) = 0, \quad \boldsymbol{x}\in\Omega \tag{16}$$

where $\mathcal{C}_{ijk} = \langle\psi_i(\boldsymbol{\xi})\psi_j(\boldsymbol{\xi}), \psi_k(\boldsymbol{\xi})\rangle_{\mu}$ denotes the inner product over the appropriate probability measure space. The probability measure μ within the integration is determined by the PDF of the random variables used. By using numerical quadrature to evaluate the inner product $\mathcal{C}_{ijk}$ [47], [55], [62], with the appropriate boundary conditions (discussed in Section II-B-II), the system reduces to a large linear combination of elliptic equations for the coefficients $\tilde{u}_j(\boldsymbol{x})$. Since the unknowns are now only functions

of space, standard finite element techniques can be employed to transform this into a large linear system of deterministic stiffness equations and right-hand-side vectors.

2) Implementation Details: In this study, we systematically investigated the effect of conductivity variability by individually perturbing the conductivity values of the organ groups within a two-dimensional cross section of the human torso, assuming uniform distributions for the conductivity variability. For the polynomial set $\{\psi_i\}$, we employed the Legendre polynomials defined on $[-1,1]$, as these are most efficient for expressing random processes with uniform (or nearly uniform) distributions.

Under these assumptions, we express the conductivity as follows:

$$\sigma(\boldsymbol{x};\boldsymbol{\xi}) = \tilde{\sigma}_0(\boldsymbol{x})\psi_0(\boldsymbol{\xi}) + \tilde{\sigma}_1(\boldsymbol{x})\psi_1(\boldsymbol{\xi}) \tag{17}$$

where $\sigma(\boldsymbol{x};\boldsymbol{\xi})$ is uniformly distributed on the interval $[a(x), b(x)]$ for each point $x \in \Omega$. We have then $\tilde{\sigma}_0(\boldsymbol{x}) = 0.5(a(\boldsymbol{x}) + b(\boldsymbol{x}))$ and $\tilde{\sigma}_1(\boldsymbol{x}) = 0.5(b(\boldsymbol{x}) - a(\boldsymbol{x}))$. Under our assumptions, only two terms are needed to represent the randomness of the conductivity. This does not imply that two polynomial chaos terms are sufficient to represent the random (and possibly non-uniformly distributed) process denoting the potential in the torso; the number of terms utilized to represent the stochastic processes is denoted P. Because we were interested in perturbing organ groups individually, we set the first mode $\tilde{\sigma}_0(\boldsymbol{x})$ to the prescribed (deterministic) value for each organ over all computational experiments. We then set $\tilde{\sigma}_1(x)$ to a nonzero value (corresponding to the half length of the uniform interval) for the organ group of interest and set $\tilde{\sigma}_1(x) = 0$ for each of the remaining organs. For example, with a 50% uniform interval, conductivity for that organ varied from 0.5 to 1.5 times that nominal (deterministic) value with equal probability of any value in that range.

Under the assumption that the boundary conditions were known and had no stochastic variability (i.e., were deterministic), the system of equations reduces to the following (for $i = 0, 1,\ j = 0, \ldots, P$):

$$\tilde{u}_0(\boldsymbol{x}) = u_0(\boldsymbol{x}), \quad \boldsymbol{x} \in \Gamma_D \tag{18}$$

$$\tilde{u}_j(\boldsymbol{x}) = 0, \quad \boldsymbol{x} \in \Gamma_D \tag{19}$$

$$\vec{n} \cdot \sigma_i(\boldsymbol{x})\boldsymbol{\nabla}\tilde{u}_j(\boldsymbol{x}) = 0, \quad \boldsymbol{x} \in \Gamma_N \tag{20}$$

with the appropriate boundary conditions (given in Section II-B2).

Equations (16) and (18)–(20) comprise a large deterministic system. To make concrete the form of this system under our assumptions, let $\mathbf{S}_0$ and $\mathbf{S}_1$ denote the stiffness matrices generated with $\tilde{\sigma}_0(\boldsymbol{x})$ and $\tilde{\sigma}_1(\boldsymbol{x})$ respectively, and let $\vec{f}_{0j}$ and $\vec{f}_{1j}$ denote the right-hand-side vectors based upon boundary conditions for $\tilde{u}_j(\boldsymbol{x})$ corresponding to $\tilde{\sigma}_0(\boldsymbol{x})$ and $\tilde{\sigma}_1(\boldsymbol{x})$, respectively. The linear system of equations that results is

$$\sum_{j=0}^{P} [\mathcal{C}_{ij0}\mathbf{S}_0 + \mathcal{C}_{ij1}\mathbf{S}_1]\,\vec{\tilde{u}}_j = \sum_{j=0}^{P} \left[\mathcal{C}_{ij0}\vec{f}_{0j} + \mathcal{C}_{ij1}\vec{f}_{1j}\right] \tag{21}$$

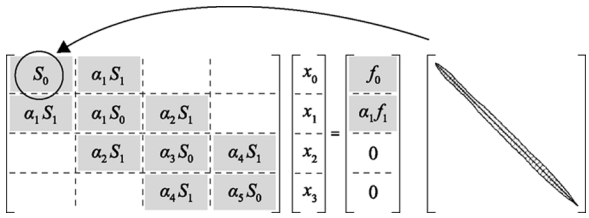

Fig. 2. Diagram of the large linear system resulting from the linear combination of stiffness matrices and right-hand sides. The α values corresponds to inner products of the stochastic basis polynomials, with $\alpha_0 = \mathcal{C}_{000}$, $\alpha_1 = \mathcal{C}_{101}$, $\alpha_2 = \mathcal{C}_{211}$, $\alpha_3 = \mathcal{C}_{220}$, $\alpha_4 = \mathcal{C}_{321}$ and $\alpha_5 = \mathcal{C}_{330}$. The matrices S_0 and S_1 are as described in the text.

for $i = 0, \ldots, P$, where $\vec{\tilde{u}}_j$ denotes the vector of finite element degrees of freedom expressing the jth stochastic mode. Given N_{dof} degrees of freedom for each finite element spatial discretization (i.e., the dimensions of the stiffness matrices $\mathbf{S}_0$ and $\mathbf{S}_1$ are N_{dof}), then the total dimension of the new stochastic linear system is $(P+1)N_{\text{dof}}$. The extension of this methodology to three spatial dimensions consists of populating the equation above with stiffness matrices and right-hand-side vectors from a three-dimensional finite element model.

Fig. 2 shows a schematic of the type of system we solved via iterative methods to obtain the stochastic moments of the solution given a third-degree stochastic Galerkin discretization (i.e., $P = 3$). Note that the choice of $P = 3$ has been made to help simplify the presentation of the figure.

3) Postprocessing: Given the stochastic modes, we calculated the mean and standard deviation of the solution as

$$\text{mean}(u(\boldsymbol{x};\xi)) = \tilde{u}_0(\boldsymbol{x})$$

$$\text{stdev}(u(\boldsymbol{x};\xi)) = \left[\sum_{i=1}^{P} (\tilde{u}_i(\boldsymbol{x}))^2 \langle \psi_i(\boldsymbol{\xi}), \psi_i(\boldsymbol{\xi})\rangle_\mu\right]^{1/2}.$$

These modes are fields over the problem domain and hence we could visualize them over the entire two-dimensional slice through the torso surface.

In all the simulations presented here, we assumed uniform distributions for the stochastic conductances and found that using stochastic polynomials of degree seven (i.e., $P = 7$) were sufficient to capture the stochastic behavior of the potentials in the torso. To verify this choice, we accomplished a comparison between Monte Carlo and the proposed methodology for one of the experiments presented in our work. We found that mean and standard deviations calculated from the simulation of 6000 Monte Carlo trials were the same to four significant figures as those computed using degree seven stochastic polynomials. However, the Monte Carlo trials required more than 2700 times the CPU time required to compute the same result using the proposed methodology. This performance discrepancy would be further exacerbated in the case of an even larger number of Monte Carlo trials.

III. Results

We present here results of a sensitivity analysis of variations in organ conductivity in a two-dimensional model of the human thorax. The epicardial potentials applied to the inner boundary

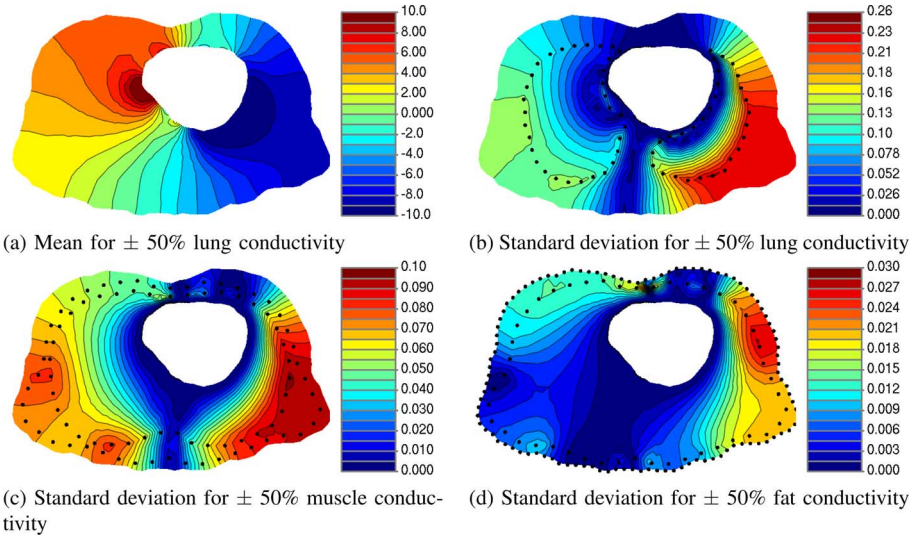

(a) Mean for ± 50% lung conductivity

(b) Standard deviation for ± 50% lung conductivity

(c) Standard deviation for ± 50% muscle conductivity

(d) Standard deviation for ± 50% fat conductivity

Fig. 3. Effects of stochastic variation in conductivities of three organs on torso potentials: These contour plots correspond to the stochastic behavior of the electrical potential across a slice through the torso resulting from stochastic organ conductivities. (a) shows the mean for a stochastic interval of ±50% from the reference lung conductivity, while (b) shows the associated standard deviation. The bottom two panels show the standard deviation for 50% stochastic variation in (c) muscle and (d) fat, respectively. In each figure depicting the standard deviation of torso potentials, the region of varying conductivity is indicated by the dotted contours. All units in the plot are millivolts.

are taken from measurements on an exposed human heart during surgery for resolution of persistent ventricular arrhythmias. For this report, we selected a time instant late (85 ms after onset) in the QRS complex as representative and present plots of mean and standard deviation of computed potential on the geometric model oriented in the standard radiological view (looking from the feet toward the head with the subject facing upward). For all of the results, we examine conductivity intervals of ±50% or smaller, as these ranges fall well within the distributions of experimentally obtained values [4]–[6].

Fig. 3 shows results for variations of 50% in the conductivity of lung, muscle and fat. Panel (a) shows the mean potentials resulting from variations in lung conductivity. As expected, the mean behavior was virtually identical for all organ conductivity experiments. The roughly dipolar nature of the epicardial boundary conditions and the similarly dipolar but considerably smoothed potential distribution on the torso surface are also evident in this figure. Such attenuation and smoothing is evident when comparing the two distinct maxima of the right ventricular potentials that fuse into a single maximum as the current travels out to the torso surface. Panels (b)–(d) show the spatial distribution of standard deviation over the thorax for variations in each of the three major organs. For variations in lung conductivity, there is a large region of high standard deviation (0.21–0.23 mV)—the highest standard deviation values for any simulation experiments at the 50% level—over the left posterolateral region of the thorax. The same region showed maximal standard deviation for variations in muscle conductivity but at a value less than half that seen for variations in lung conductivities. Variations in lung conductivity also produced elevated but submaximal standard deviations in the region on the right posterolateral aspects of the thorax, a region once again shared (albeit at relatively lower amplitudes) in the results for variation in muscle conductivity. In contrast, for variations in subcutaneous fat conductivity, only one region located in left anterolateral area showed elevated standard deviation values and even there, the amplitude was an order of magnitude smaller (0.03 mV) than the maximum for variations in lung conductivity.

We performed experiments with artificially rotated epicardial potentials to determine the effect of epicardial potential orientation on variations in torso potential and standard deviation. Fig. 4 shows one such example in which panel (a) contains mean results for a 90° rotation in epicardial potentials relative to those shown in Fig. 3. The associated patterns of standard deviation shifted in response to the altered epicardial potentials but not in a way that reflected a simple rotation. For example, a comparison of panel (d) in both figures, both showing the standard deviation from a 50% variation in fat conductivity, shows that for the original orientation, a single area of elevated standard deviation exists (Fig. 3), while rotating the same potentials resulted in three widely separate regions of elevated standard deviation (Fig. 4).

Fig. 4 also illustrates the effect of scaling on sensitivity of torso potentials to variations in conductivity. Panels (b) and (c) appear almost identical in pattern but amplitudes vary by a factor of approximately 5, equal to the ratio of the respective range of variation in conductivity (50% versus 10%).

Another finding shown in Fig. 4 is the nature of interactions between variations of conductivity in multiple organs. Panels (b)–(d) show standard deviations for variations in a single organ while panels (e) and (f) show results from allowing simultaneous variation of both lung and fat conductivity. We selected a level of variation for each component that generated approximately equal individual variance in the forward solutions; the combined effects are certainly a function of the relative levels of variation in the individual parameters. In one combined case, panel (e), conductivities are coupled through a single random variable while in the other case, panel (f), variations are functions of two independent variables. In both instances, there are features in the maps of cumulative standard deviation that ap-

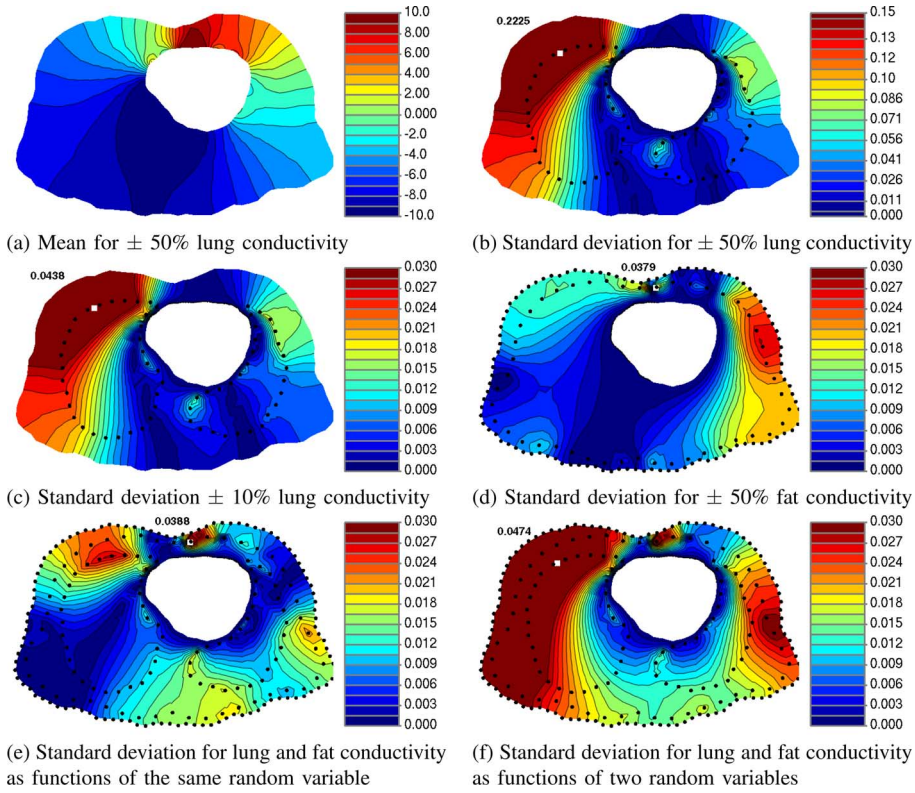

(a) Mean for ± 50% lung conductivity

(b) Standard deviation for ± 50% lung conductivity

(c) Standard deviation ± 10% lung conductivity

(d) Standard deviation for ± 50% fat conductivity

(e) Standard deviation for lung and fat conductivity as functions of the same random variable

(f) Standard deviation for lung and fat conductivity as functions of two random variables

Fig. 4. Effects of multiple stochastic dimensions on the variance of the torso potentials: These contour plots correspond to the stochastic behavior of the electrical potential across the torso surface resulting from stochastic conductivity with uniform distribution where the epicardial potentials have been rotated clockwise 180°. (a) shows the mean torso potentials for stochastic lung conductivity with values varying within $\pm 50\%$ from the reference value, while (b) depicts the standard deviation. (c) depicts the standard deviation for stochastic lung conductivity of $\pm 10\%$ as a function of a single random variable. (d) depicts the standard deviation for stochastic fat conductivity of $\pm 50\%$ as a function of a single random variable. (e) depicts the standard deviation for stochastic lung conductivity of $\pm 10\%$ and stochastic fat conductivity of $\pm 50\%$ where both stochastic lung and fat are a function of the same single random variable. (f) depicts the results of stochastic lung and fat conductivity variation from the same components as in (e), but each is a function of two independent and uncorrelated random variables. In each figure depicting the standard deviation of torso potentials, the region of varying conductivity is indicated by the dotted contours. The numerical value of the maximum is included in each plot and all units in the plot are millivolts.

pear to originate from one or the other of the associated single-parameter maps. However, the cumulative distributions are not simple algebraic sums of the single-parameter distributions, indicating complex interactions between the conductivities of different organs. Another finding illustrated in the figure was the larger standard deviations of potential resulting from independent variation of multiple conductivities as compared to variations linked to a single random variable.

IV. Discussion

The main purpose of this study was to present a novel approach to parameter sensitivity analysis that could have application to a wide range of bioelectric and biomedical simulation problems.

A thorough sensitivity analysis as described here has distinct advantages over the approaches used in most previously reported studies that have sought to establish the effects of conductivity variation on forward ECG and EEG problems [7], [10]. Most notably, rather than investigating only a small subset of model parameter value combinations, in a full statistical analysis one is able to explore the impact of a continuous range of organ conductivity values on torso potentials. In addition, this approach provides a complete spatial distribution of the effects of parameter variation on the forward solution rather than a single value (typically the root mean squared of the difference between solutions) as with most other investigations of this type. Thus, it is possible to observe that variations in organ regions result in standard deviations with widely different spatial distributions as illustrated by Figs. 3 and 4. Analysis of these spatial patterns, in turn, can suggest a correspondence between the effect of source potentials, problem domain geometry, and the location and value of the conductivity variations upon the resulting potentials throughout the problem domain. It is these relationships that reveal features of, in this case, the electrocardiographic forward problem and its implementation under realistic conditions.

Although we do not report on a complete sensitivity analysis of the forward problem, there are some observations that illustrate the utility of the stochastic approach—observations that are not possible using the more typical analyses from past studies.

As an example of the insights stochastic analysis can provide, we noted that the mean potentials across the torso cross section were extremely similar for multiple distributions of organ conductivities. This finding is expected due to the symmetry of the conductivity probability distributions examined and the relatively linear behavior of the elliptic problem with respect to the conductivities. In contrast, we noted distinct differences in the spatial distribution of the standard deviations for variations in

conductivity of the various organs. By generating spatial distribution of mean potential and standard deviation over the entire cross section, we were able to observe the relationship between these parameters and the geometry of the organ boundaries and thus visualize the effects of changing conductivities. For example, Fig. 3 shows that the structure of mean potential [shown in (a)] did not obviously reflect underlying organ boundaries whereas maps of standard deviation in (b) and (c) show breaks in the iso-value lines that align with the boundary of the lungs and muscle, respectively. The standard deviation from variation in subcutaneous fat [depicted in (d)] shows a weaker association with internal organ boundaries.

Our findings appear to contradict those of Klepfer *et al.*, who determined that both skeletal muscle and fat conductivities had greater affect than lung conductivity on the three-dimensional forward problem of electrocardiography [7]. These findings, however, were based on the assumption of skeletal muscle anisotropy; indeed, in the case of isotropic skeletal muscle conductivities (as were used in our study), the effects of muscle conductivity were significantly less than for lung conductivities. The fat conductivities have elevated impact in the study by Klepfer *et al.*, perhaps because the difference between the two fat conductivity values investigated was significantly larger than the intervals examined here. A full comparison of results will require the use of equivalent, three-dimensional models.

The accuracy of a geometric model depends not only on conductvity values but also—and perhaps even more so—on the proximity of the various organs to the bounding surfaces of the problem and the geometric accuracy of the regions of different conductivity. The stochastic approach we describe here is also suited to an analysis of such geometric variation, a project beyond the scope of this report. Ultimately, one would like to allow variation in both conductivity and geometry and determine the influence of these variations on the forward solution. To address the question of the role of anisotropy of the skeletal muscle described by Klepfer *et al.* [7] would then require an additional parameter in the variational analysis. Conceptually, all this is possible using our approach—conversely, the computational cost of any of the more traditional approaches of sensitivity analyses would become all the more insurmountable if one were to vary all the relevant parameters simultaneously.

Orientation of the epicardial potentials greatly affected the spatial characteristics of both the mean potentials and especially their standard deviation. Figs. 3 and 4 illustrate these effects for epicardial potentials rotated by approximately 90°, as shown in panel (a) of both figures. The effect of rotation on mean potential was predictably a rotation of the same pattern, slightly distorted by the asymmetric shape of the torso cross section. The effect on standard deviation was, however, markedly more complex, indicating a more complex relationship between potential distribution and placement of the regions of different conductivity. At this point, it is difficult to draw many general conclusions about this relationship but it does appear that the organ conductivities impact the potentials most significantly when they are located in close proximity to regions of large amplitudes of epicardial potentials. Such regions of large source strength induce large current flow and one can expect this flow to change most in regions of large conductivity change. In addition, we noted that the regions of greatest standard deviation did not necessarily occur at the organ boundaries or even within the large organs, but rather near the torso boundary itself. Such findings suggest a form of remote effect, i.e., changes in conductivity in one region alter most strongly the potentials in another region, perhaps because in these regions, the current has already passed through large regions of changing conductivity and the cumulative effects of deflection and attenuation have grown.

We also observed that the combined effect of conductivity variations in two different organs is not additive, and thus cannot be predicted by the individual stochastic behavior of single organ regions. We found that standard deviation for combinations of stochastic organs was typically larger than for the individual organs, suggesting that in concert, errors are compounded. Moreover, although some features of the standard deviation distribution from combined variation were present in one or the other of the equivalent maps of the individual variations, there were also unique features only visible in the combined distribution. These findings emphasize the importance of quantifying the collective (rather than individual) impact of organ conductivities upon the full model and further underscore the value of the gPC-SG method in enabling such forms of analysis.

The studies presented here were based on a two-dimensional simplification of a three-dimensional problem. The gPC-SG approach is not intrinsically limited to two dimensions and for this forward problem extends naturally to three, as outlined briefly in Section II. The simplification from three to two dimensions also necessitates care in interpreting the findings as they apply to this problem and especially the importance of extending them to a full, three-dimensional model. One obvious effect of the simple model was that computed torso surface potentials were larger than what one would expect from a three-dimensional model. This is clearly a result of the reduced torso volume relative to the extent of the epicardial sources, which decreases the electrical load on the source potentials and thus increases the potential amplitude throughout the cross section. One cannot reliably speculate upon the equivalent change in amplitude of standard deviations in a three-dimensional model, although the linearity of the problem suggests the likelihood of similar scaling. We do note that the patterns visible in the cross section generally projected more or less radially to the outer boundary (the torso surface contour). However, the effect of a three-dimensional model on spatial distributions of standard deviation is difficult to anticipate and awaits the results from ongoing studies in our laboratory with three-dimensional implementations of this approach.

While we present a gPC-SG analysis of the influence of conductivity on a specific problem in electrocardiography, this approach can be extended to a number of other biological problems, including that of source localization in the brain from extracranial measurements of electric potentials or magnetic fields. Technical hurdles have previously made this sort of analysis prohibitive due to the large number of samples necessary or the complexity of implementation. The gPC-SG approach provides a framework capable of overcoming these hurdles. The computational tractability of gPC-SG also allows for investigating the effects of multiple stochastic parameters

or even multiple random-dimensional stochastic parameters in a reasonable amount of time.

ACKNOWLEDGMENT

The authors would like to thank Dr. D. Xiu of Purdue University, West Lafayette, IN, for his generous help introducing us to generalized polynomial chaos, Dr. T. Preusser of University of Bremen, Germany, for his comments concerning presentation of the material, and S. Choe for providing the two-dimensional finite element solver used in this paper. The authors also acknowledge the computational support and resources provided by the Scientific Computing and Imaging Institute. Support for the acquisition of the data used within the simulation studies came from the Nora Eccles Treadwell Foundation.

REFERENCES

[1] R. M. Gulrajani, F. A. Roberge, and G. E. Mailloux, "The forward problem of electrocardiography," in *Comprehensive Electrocardiology*, P. W. Macfarlane and T. D. Veitch Lawrie, Eds. Oxford, U.K.: Pergamon, 1989, pp. 197–236.

[2] R. M. Gulrajani, "The forward and inverse problems of electrocardiography," *EMBS Mag.*, vol. 17, no. 5, pp. 84–101, 1998.

[3] R. S. MacLeod and D. H. Brooks, "Recent progress in inverse problems in electrocardiology," *IEEE Eng. Med. Biol. Mag.*, vol. 17, no. 1, pp. 73–83, Jan. 1998.

[4] F. A. Duck, *Physical Properties of Tissue: A Comprehensive Reference Book*. London, U.K.: Academic/Harcourt Brace Jovanovich, 1990.

[5] C. Gabriel, S. Gabriel, and E. Corthout, "The dielectric properties of biological tissue: I. literature survey," *Phys. Med. Biol.*, vol. 41, pp. 2231–2249, 1996.

[6] T. J. Faes, H. A. van der Meij, J. C. de Munck, and R. M. Heethaar, "The electric resistivity of human tissues (100 Hz – 10 Mhz): A meta-analysis of review studies," *Physiol. Meas.*, vol. 20, pp. R1–R10, 1999.

[7] R. N. Klepfer, C. R. Johnson, and R. S. MacLeod, "The effects of inhomogeneities and anisotropies on electrocardiographic fields: A three-dimensional finite elemental study," in *Proc. 17th Annu. IEEE Engineering Medicine Biology Soc. Int. Conf.*, 1995, pp. 233–234.

[8] C. R. Johnson, R. S. MacLeod, and A. Dutson, "Effects of anistropy and inhomogeneity on electrocardiographic fields: A finite element study," in *Proc. 14th Annu. IEEE Engineering Medicine Biology Soc. Int. Conf.* , 1992, pp. 2009–2010.

[9] C. R. Johnson, R. S. MacLeod, and P. R. Ershler, "A computer model for the study of electrical current flow in the human thorax," *Comput. Biol. Med.*, vol. 22, no. 3, pp. 305–323, 1992.

[10] M. L. Buist and A. J. Pullan, "The effect of torso impedance on epicardial and body surface potentials: A modeling study," *IEEE Trans. Biomed. Eng.*, vol. 50, no. 7, pp. 816–824, Jul. 2003.

[11] G. J. M. Huiskamp and A. van Oosterom, "The effect of torso inhomogeneities on body surface potentials," *J. Electrocardiol.*, vol. 22, pp. 1–20, 1989.

[12] A. van Oosterom and G. J. Huiskamp, "The effect of torso inhomogeneities on body surface potentials quantified using "tailored" geometry," *J. Electrocardiol.*, vol. 22, pp. 53–72, 1989.

[13] A. Pullan, "The inverse problem of electrocardiography: Modeling, experimental, and clinical issues," *Biomed. Technik*, vol. 46, pp. 197–198, 2001, supplement.

[14] S. E. Geneser, S. Choe, R. M. Kirby, and R. S. Macleod, "The influence of stochastic organ conductivity in 2-D ECG forward modeling: A stochastic finite element study," in *Proc. 27th Annu. IEEE Eng. Medicine Biology Conf.*, Shanghai, China, Sep. 1–4, 2005, pp. 5528–5531.

[15] S. E. Geneser, S.-K. Choe, R. M. Kirby, and R. S. Macleod, "2D stochastic finite element study of the influence of organ conductivity in ECG," *Int. J. Bioelectromagn.*, vol. 7, no. 1, pp. 321–324, 2005.

[16] S. E. Geneser, D. B. Xiu, R. M. Kirby, and F. B. Sachse, "Stochastic Markovian modeling of electrophysiology of ion channels: Reconstruction of standard deviations in macroscopic currents," *J. Theor. Biol.*, vol. 245, no. 4, pp. 627–637, 2007.

[17] R. Tomovic, *Sensitivity Analysis of Dynamic Systems*. New York: McGraw-Hill, 1963.

[18] L. Radanovic, *Sensitivity Methods in Control Theory*. Oxford, U.K.: Pergamon, 1966.

[19] P. M. Frank, *Introduction to System Sensitivity*. New York: Academic, 1978.

[20] G. I. Schueller, "Computational stochastic mechanics – Recent advances," *Comput. Struct.*, vol. 79, pp. 2225–2234, 2001.

[21] C. W. Bullard and A. V. Sebald, "Monte Carlo sensitivity analysis of input-output models," *Rev. Econ. Statistics*, vol. 70, pp. 708–712, 1988.

[22] C. P. Robert and G. Casella, *Monte Carlo Statistical Methods*. New York: Springer, 1999.

[23] R. L. Iman and W. J. Conover, "Small sample sensitivity analysis techniques for computer models, with an application to risk assessment," *Commun. Stat. Theory Meth.*, vol. A9, no. 17, pp. 1749–1842, 1980.

[24] J. C. Helton, F. J. Davis, and J. D. Johnson, "A comparison of uncertainty and sensitivity analysis results obtained with random and Latin hypercube sampling," *Reliab. Eng. Syst. Saf.*, vol. 89, pp. 305–330, 2005.

[25] R. H. Myers and D. C. Montgomery, *Response Surface Methodology: Process and Product in Optimization Using Designed Experiments*. New York: Wiley, 1995.

[26] R. Lu, Y. Luo, and J. P. Conte, "Reliability evaluation of reinforced concrete beam," *Struct. Saf.*, vol. 14, pp. 277–298, 1994.

[27] A. Karamchandani and C. A. Cornel, "Sensitivity estimation within first and second order reliability methods," *Struct. Saf.*, vol. 11, pp. 95–107, 1992.

[28] G. J. McRae, J. W. Tilden, and J. H. Seinfeld, "Global sensitivity analysis—A computational implementation of the Fourier amplitude sensitivity test (FAST)," *Comput. Chem. Eng.*, vol. 6, pp. 15–25, 1982.

[29] S. Seigneur, T. W. Teche, R. M. Roth, and L. E. Reid, "Sensitivity of complex urban air quality model to input data," *J. Appl. Meteorol.*, vol. 20, pp. 157–177, 1981.

[30] J. C. Dechaux, V. Zimmerman, and V. Nollet, "Sensitivity analysis of the requirements of rate coefficients for the operational models of photochemical oxidants formation in the troposphere," *Atmosph. Environ.*, vol. 28, pp. 195–211, 1994.

[31] R. R. Dickerson, D. H. Stedman, and A. C. Delany, "Direct measurements of ozone and nitrogen dioxide photolysis rates in the troposphere," *J. Geophys. Res.*, vol. 87, pp. 4933–4946, 1982.

[32] E. P. Doughtery and H. Rabitz, "A computational algorithm for the Green's function method of sensitivity analysis in chemical kinetics," *Int. J. Chem. Kinet.*, vol. 11, pp. 1237–1249, 1979.

[33] E. P. Doughtery, J. T. Hwang, and H. Rabitz, "Further developments and applications of the Green's function method of sensitivity analysis in chemical kinetics," *Int. J. Chem. Kin.*, vol. 71, pp. 1794–1808, 1979.

[34] G. Adomian, *Applied Stochastic Processes*. New York: Stochastic System Analysis, 1980, pp. 1–17.

[35] O. Baysal and M. E. Eleshaky, "Aerodynamic design optimization using sensitivity analysis and computational fluid dynamics," *Amer. Inst. Aeron. Astron.*, vol. 30, no. 3, pp. 718–725, 1992.

[36] D. M. Hamby, "A review of techniques for parameter sensitivity analysis of environmental models," *Environ. Monitor. Assess.*, vol. 32, no. 2, pp. 135–154, 1994.

[37] J. M. Holtzman, "On using perturbation analysis to do sensitivity analysis: Derivatives versus differences," in *Proc. 28th IEEE Conf. Decision Control*, Tampa, FL, Dec. 13–15, 1989, pp. 2018–2023.

[38] H. Feild and K. Emery, "An uncertainty analysis of the spectral correction factor," in *Conf. Rec. 23rd IEEE Photovoltaic Specialists Conf.*, Louisville, KY, May 10–14, 1993, pp. 1180–1187.

[39] B. W. Lee and O. K. Lim, "Application of the first-order perturbation method to optimal structural design," *Struct. Eng. Mechan.*, vol. 4, pp. 425–436, 1996.

[40] N. Wiener, "The homogeneous chaos," *Amer. J. Math.*, vol. 60, no. 4, pp. 897–936, 1938.

[41] W. C. Meecham and D. T. Jeng, "Use of Wwiener-Hermite expansion for nearly normal turbulence," *J. Fluid Mech.*, no. 32, pp. 225–249, 1968.

[42] A. J. Chorin, "Hermite expansions in Monte Carlo computation," *J. Comput. Phys.*, vol. 8, pp. 471–482, 1971.

[43] A. J. Chorin, "Gaussian fields and random flow," *J. Fluid Mech.*, vol. 63, pp. 21–32, 1974.

[44] F. H. Maltz and D. L. Hitzl, "Variance reduction in Monte Carlo computations using multi-dimensional Hermite polynomials," *J. Comput. Phys.*, vol. 32, pp. 345–376, 1979.

[45] M. K. Deb, I. M. Babuška, and J. T. Oden, "Solutions of stochastic partial differential equations using Galerkin finite element techniques," *Comput. Methods Appl. Mech. Eng.*, vol. 190, pp. 6359–6372, 2001.

[46] O. P. Le Maître, M. Reagan, H. N. Najm, R. G. Ghanem, and O. M. Knio, "A stochastic projection method for fluid flow II: Random process," *J. Comput. Phys.*, vol. 181, no. 1, pp. 9–44, 2002.

[47] D. B. Xiu and G. E. Karniadakis, "Modeling uncertainty in steady state diffusion problems via generalized polynomial chaos," *Comput. Methods Appl. Mech. Eng.*, vol. 191, pp. 4927–4948, 2002.
[48] D. B. Xiu and G. E. Karniadakis, "Modeling uncertainty in flow simulations via generalized polynomial chaos," *J. Comput. Phys.*, vol. 187, pp. 137–167, 2003.
[49] D. Lucor, C.-H. Su, and G. E. Karniadakis, "Generalized polynomial chaos and random oscillators," *Int. J. Numer. Meth. Eng.*, vol. 60, pp. 571–596, 2004.
[50] R. G. Ghanem, "Higher order sensitivity of heat conduction problems to random data using the spectral stochastic finite element method," *ASME J. Heat Transfer*, vol. 121, pp. 290–299, 1999.
[51] V. A. Narayanan and N. Zabaras, "Stochastic inverse heat conduction using a spectral approach," *Int. J. Numer. Meth. Eng.*, vol. 60, pp. 1569–1593, 2004.
[52] D. B. Xiu and G. E. Karniadakis, "A new stochastic approach to transient heat conduction modeling with uncertainty," *Int. J. Heat Mass Transfer*, vol. 46, pp. 4681–4693, 2003.
[53] M. T. Reagan, H. N. Najm, B. J. Debusschere, O. P. Le Maître, O. M. Knio, and R. G. Ghanem, "Spectral stochastic uncertainty quantification in chemical systems," *Combust. Theory Model.*, vol. 8, pp. 607–632, 2004.
[54] M. T. Reagan, H. N. Najm, P. P. Pébay, O. M. Knio, and R. G. Ghanem, "Quantifying uncertainty in chemical systems modeling," *Int. J. Chem. Kin.*, vol. 37, pp. 386–382, 2005.
[55] R. G. Ghanem and P. Spanos, *Stochastic Finite Elements: A Spectral Approach*. New York: Springer-Verlag, 1991.
[56] T. J. R. Hughes, *The Finite Element Method: Linear Static and Dynamic Finite Element Analysis*. Mineola, NY: Dover, 2000.
[57] B. A. Szabó and I. M. Babuška, *Finite Element Analysis*. New York: Wiley, 1991.
[58] G. E. Karniadakis and S. J. Sherwin, *Spectral/HP Element Methods for CFD*. New York: Oxford Univ. Press, 1999.
[59] O. Axelsson, *Iterative Solution Methods*. Cambridge, U.K.: Cambridge Univ. Press, 1994.
[60] R. S. MacLeod, C. R. Johnson, and P. R. Ershler, "Construction of an inhomogeneous model of the human torso for use in computational electrocardiography," in *Proc. 13th Annu. Int. Conf. IEEE Eng. Medicine Biology Soc.*, 1991, pp. 688–689.
[61] R. N. Klepfer, C. R. Johnson, and R. S. MacLeod, "The effects of inhomogeneities and anisotropies on electrocardiographic fields: A three-dimensional finite element study," *IEEE Trans. Biomed. Eng.*, vol. 44, no. 8, pp. 706–719, 1997.
[62] D. B. Xiu and G. E. Karniadakis, "The Wiener-Askey polynomial chaos for stochastic differential equations," *SIAM J. Sci. Comput.*, vol. 24, pp. 619–644, 2002.
[63] M. Loève, *Probability Theory I*, 4th ed. New York: Springer-Verlag, 1977.
[64] I. M. Babuška, R. Tempone, and G. E. Zouraris, "Galerkin finite element approximations of stochastic elliptic differential equations," *SIAM J. Numer. Anal.*, vol. 42, pp. 800–825, 2004.
[65] O. P. Le Maître, O. M. Knio, H. N. Najm, and R. G. Ghanem, "Uncertainty propagation using Wiener-Haar expansions," *J. Comput. Phys.*, vol. 197, pp. 28–57, 2004.

Sarah E. Geneser received the M.A. degree in mathematics from the University of Utah, Salt Lake City, in 2002. She is currently working toward her Ph.D. degree in computer science at the University of Utah.

She is a member of the Scientific Computing and Imaging Institute at Utah, and her research interests lie in scientific computing.

Robert M. Kirby (M'02) received the M.S. degree in applied math, the M.S. degree in computer science, and the Ph.D. degree in applied mathematics from Brown University, Providence, RI, in 1999, 2001, and 2002, respectively.

He is an Assistant Professor of computer science at the School of Computing, an Adjunct Assistant Professor in the Department of Bioengineering, and a member of the Scientific Computing and Imaging Institute, all at the University of Utah, Salt Lake City. His research interests lie in scientific computing and visualization.

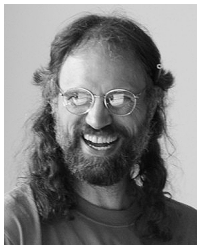

Robert S. MacLeod (S'87–M'87) received the B.S. degree in engineering physics from Dalhousie University, Halifax, NS, Canada, in 1979, the M.S. degree in electrical engineering from the Technische Universität, Graz, Austria, in 1985, and the Ph.D. degree in physiology and biophysics from Dalhousie University in 1990.

He is an Associate Professor in the Bioengineering Department and the Department of Internal Medicine (Division of Cardiology) at the University of Utah, Salt Lake City, where he is an Associate Director of the Scientific Computing and Imaging Institute, the Nora Eccles Harrison Cardiovascular Research and Training Institute, and the Department of Bioengineering. His research interests include computational electrocardiography (forward and inverse problems), experimental investigation and clinical detection of cardiac ischemia and repolarization abnormalities, cardiac imaging in atrial fibrillation, and scientific computing and visualization.